International Journal of Power Electronics and Drive System (IJPEDS)
Vol. 10, No. 3, Sep 2019, pp. 1197~1206
ISSN: 2088-8694, DOI: 10.11591/ijpeds.v10.i3.1197-1206

Performance evaluation of multi-phase permanent magnet synchronous motor based on different winding configurations and magnetization patterns

M. Rezal[1], D. Ishak[2]
[1] Universiti Kuala Lumpur, Malaysian Spanish Institute, Malaysia
[2] School of Electrical & Electronic Engineering, Universiti Sains Malaysia

Article Info

Article history:

Received Jul 17, 2018
Revised Feb 14, 2019
Accepted Mar 25, 2019

Keywords:

Permanent magnet
Synchronous motor
Magnetization pattern
Winding configuration
Skewing method

ABSTRACT

Permanent magnet synchronous motor (PMSM) is the most reliable and efficient machine that widely used in robotics and automation, industrial applications, electric vehicles, home appliances, aircraft and aerospace technology due to its high efficiency, good dynamic performance and high torque density. In this paper, the influence of various types of winding configuration and different magnetization patterns in the performance of a five-phase PMSM is investigated. Three types of magnetization patterns such as radial magnetization (RM), parallel magnetization (PaM), and multi-segmented Halbach magnetization (SH) are applied to the five-phase 10-slot/4-pole PMSM during open-circuit and on-load conditions. A 2D finite element method (FEM) is intensively used in this investigation to model and predict the electromagnetic characteristics and performance of the PMSM. The detailed results from the finite-element analysis (FEA) on the cogging torque, induced back-emf, airgap flux density and electromagnetic torque are analysed. The induced back-emf of the machine is computed further into its harmonic distortions. Additionally, the skewing method for minimization of cogging torque of PMSM is proposed. From the results, it is observed that the five-phase, 10-slot/4-pole PMSM with double layer distributed winding and parallel magnetization gives the best machine performance.

Corresponding Author:

Dahaman Ishak,
School of Electrical and Electronic Engineering,
Universiti Sains Malaysia,
14300 Nibong Tebal, Penang, Malaysia.
Email: dahaman@usm.my

1. INTRODUCTION

For the past decades, transportation sector's fuel consumption has grown at a higher rate than other industrial sectors. This increase was largely derived from the new demand for personal use of vehicles powered by conventional internal combustion engines. With increased awareness of air pollutions and rising fuel prices, electric vehicles have emerged as an alternative solution to replace the conventional vehicles [1, 2]. Permanent magnet synchronous motor (PMSM) is a very good candidate for the electric vehicle applications due to its advantages such as high power density and high efficiency with an efficient heat lost to the surrounding [3, 4]. However, electric vehicle applications require extremely high reliability that made the traditional three-phase PMSM facing a severe challenge. Multi-phase drives have additional degrees of freedom that can be used for different purposes, such as additional torque generation or fault tolerance when a part of the system fails [5-7]. With the increase in the number of phases, the multi-phase PMSM can obtain the highest possible reliability. Therefore, multi-phase PMSM drive system offers another solution for the electric vehicle drive system. In order to achieve a high performance PMSM, both rotor and stator structures

of the motor must be considered. PMSM has two types of windings which can be applied to the stator core such as concentrated windings and distributed windings [8, 9]. The concentrated windings can reduce the copper loss, while the distributed windings may contribute to higher torque output of the motor. But the copper loss from distributed windings is usually higher than that of concentrated windings. In this paper, a five-phase, 10-slot/4-pole PMSM is designed based on an analytical calculation to determine the machine dimensions using sizing equations. The machine performance is modelled using analytical sub-domain model, and further analysed using the finite element method that involves with three different winding types i.e. double-layer distributed winding (DLDW), single-layer concentrated winding (SLCW), and double-layer concentrated winding (DLCW). Three types of magnetization patterns such as radial magnetization (RM), parallel magnetization (PaM) and segmented Halbach (SH) magnetization are also considered for this five=phase, 10-slot/4-pole PMSM. The influences of winding configurations and magnetization patterns on the phase back-emf and the electromagnetic torque are analyzed and compared. Additionally, the cogging torque is analysed and further minimized by applying the stator skewing method. The machine model with the best machine performance will be selected. The research starts by determining the machine design parameters using an analytical model and sizing equations. Then, six models of PMSM that have different magnetization patterns and winding configurations are developed. The PMSM motor performances i.e. the magnetic vector potential, flux density distribution, phase back-emf, cogging torque, and electromagnetic torque for each design are analyzed. Finally, a skewing method is applied in order to reduce the cogging torque.

2. RESEARCH METHOD

2.1. Machine design parameters

The machine dimensions for the five-phase, 10-slot/4-pole PMSM are determined based on analytical calculation. In order to calculate the dimensions, some parameters are fixed to ensure this machine model is applicable in hybrid electric vehicles (HEVs) and electric vehicles (EVs). The fixed parameters for the five-phase PMSM are referred from [10] as shown in Table 1. In [10], the five-phase PMSM applied surface-mounted segmented Halbach (SH) magnetization with double-layer concentrated winding (DLCW) configuration.

Table 1. Main parameters for five-phase, 10-slot/4-pole PMSM

Parameters	Values	Parameters	Value
Magnet remanence, B_r (T)	1.10	Tooth end width, w_{te}(mm)	1.5
Saturation flux density, B_{sat} (T)	1.60	Stator bore radius, R_{si} (mm)	26
Magnet relative permeability, μ_r	1.04	Rotor outer radius, R_r (mm)	20
Axial active length, l_a(mm)	100	Shaft radius, R_{sh}(mm)	8
Air gap thickness, l_g (mm)	1	Wire diameter (mm)	1
Magnet thickness, l_m (mm)	5	Slot fill factor, k_f	0.4
Stator outer radius, R_{so}(mm)	60	Iron type	M19-29G
Magnet outer radius, R_m(mm)	25	PM type	NdFeB

The others machine parameters such as stator tooth body, stator yoke, rotor yoke, and tooth tip are identified using sizing equations [11]. The average air gap flux density B_g is determined using (1), where the symbols are defined in Table 1. Magnetic flux from the rotor magnet will cross the air gap and enter the stator teeth. Therefore, the total flux per stator tooth $\emptyset_{sp}$ is obtained using (2), where N_s is the number of slots. Assuming that saturation level of flux density B_{sat} in the stator and rotor core is not more than 1.6T, then the stator tooth body w_{tb} is calculated using (3). For this 10-slot/4-pole PMSM, the total flux passing through the stator tooth body will not split into two halves when reaching the stator yoke. Therefore, the stator yoke w_{sy} will have the same height as the stator tooth body w_{tb} as represented in (4). The rotor yoke w_{ry} is assumed higher than the theoretical value. The minimum value of rotor yoke is calculated using (5). Total flux per magnet pole $\emptyset_{rp}$ is determined using (6), where p is the pole-pair number of the PMSM. Figure 1 shows the 10-slot/4-pole PMSM model with different magnetization patterns i.e. RM, PM, and SH.The performances of machine i.e. phase back-emf and output torque are affected by the allocation of slots for the phase coils. Therefore, it is important to determine the winding arrangements in the five-phase, 10-slot/4-pole PMSM which maximizes the machine performance. The allocations of phase windings in the 10-slot/4-pole PMSM are shown in Figure 2

$$B_g = B_r/\left(1 + \mu_r l_g/l_m\right) \quad (1)$$

$$\emptyset_{sp} = 2\pi R_{si} B_g l_a/N_s \quad (2)$$

$$w_{tb} = \emptyset_{sp}/B_{sat} l_a \quad (3)$$

$$w_{sy} = w_{tb} \quad (4)$$

$$w_{ry} = \emptyset_{rp}/2B_{sat} l_a \quad (5)$$

$$\emptyset_{rp} = 2\pi R_m B_g l_a/2p \quad (6)$$

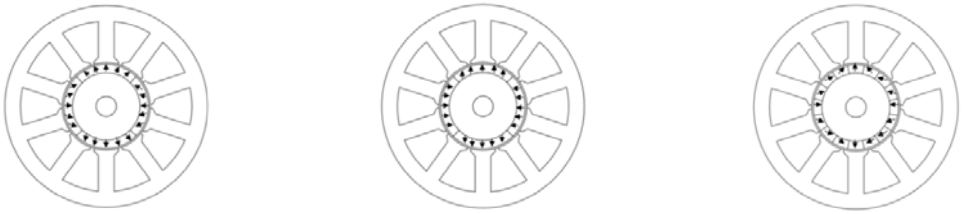

(a) (b) (c)

Figure 1. Rotor magnet with different magnetization patterns for five-phase, 10-slot/4pole PMSM, (a) Radial magnetization (RM), (b) Parallel magnetization (PaM), (c) Segmented Halbach (SH)

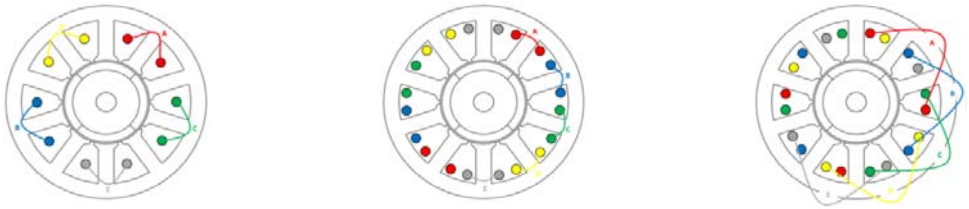

(a) (b) (c)

Figure 2. Allocation of phase windings for five-phase, 10-slot/4-pole PMSM, (a) SLCW, (b) DLCW, (c) DLDW

2.2. Analytical sub-domain model

Analytical sub-domain model applies separation of variables technique using 2D Laplace's equation for the airgap and slot opening regions, while 2D Poisson's equation for the magnet and winding slot regions [12, 13]. The airgap magnetic flux density distributions during open-circuit, armature reaction and on-load conditions can be accurately estimated using this analytical sub-domain model. The airgap magnetic flux density can be determined by applying the appropriate equations with certain boundaries. There are four regions in the motor modelling i.e. magnet, air-gap, slot opening, and winding slot as shown in Figure 3 [14-17].

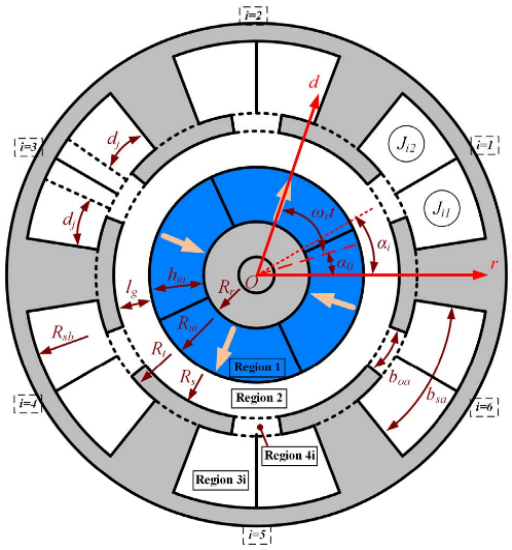

Figure 3. 2D design for analytical sub-domain model (Region 1: PM, Region 2: airgap, Region 3: slot-opening, Region 4: winding slot) [18]

The magnetic field distributions, phase back-emf, electromagnetic torque, and winding inductance can then be calculated. Few assumptions are used in formulating the analytical sub-domain model i.e. infinite permeability in the rotor and stator cores; no conductivity in the rotor and stator cores; the eddy current reaction field is neglected in this model; the teeth are spoke shaped (radial slot boundaries); end-effect is neglected; and linear magnet properties [19]. In order to simplify the analytical sub-domain modelling, in this paper, only two regions are considered, i.e. magnet region and airgap region. The magnetic flux density in the airgap is obtained analytically using (7) and (8) for its radial and tangential components respectively [20]

$$
\begin{aligned}
B_{srl}(r,\theta) = & \sum_{n=1,3,5\ldots}^{\infty} \frac{\mu_o M_n}{2\mu_r} \cdot \frac{np}{(np)^2-1} \\
& \cdot \left(\frac{2\left[\left(\frac{R_r}{R_m}\right)^{np+1} - \left(\frac{R_r}{R_m}\right)^{2np}\right]}{\frac{\mu_r+1}{\mu_r}\left[1-\left(\frac{R_r}{R_s}\right)^{2np}\right] - \frac{\mu_r-1}{\mu_r}\left[\left(\frac{R_m}{R_s}\right)^{2np} - \left(\frac{R_r}{R_m}\right)^{2np}\right]} \right) \\
& \cdot \left[\left(\frac{r}{R_s}\right)^{np-1}\left(\frac{R_m}{R_s}\right)^{np+1} + \left(\frac{R_m}{r}\right)^{np+1}\right] \cdot \cos(np\theta) \cdot \left(\lambda_0 + \sum_{n=1}^{N_\lambda} \lambda_{an} \cdot \cos(nQ_s\theta)\right) \\
& + \sum_{n=1,3,5\ldots}^{\infty} \frac{\mu_o M_n}{2\mu_r} \cdot \frac{np}{(np)^2-1} \\
& \cdot \left(\frac{2\left[\left(\frac{R_r}{R_m}\right)^{np+1} - \left(\frac{R_r}{R_m}\right)^{2np}\right]}{\frac{\mu_r+1}{\mu_r}\left[1-\left(\frac{R_r}{R_s}\right)^{2np}\right] - \frac{\mu_r-1}{\mu_r}\left[\left(\frac{R_m}{R_s}\right)^{2np} - \left(\frac{R_r}{R_m}\right)^{2np}\right]} \right) \\
& \cdot \left[-\left(\frac{r}{R_s}\right)^{np-1}\left(\frac{R_m}{R_s}\right)^{np+1} + \left(\frac{R_m}{r}\right)^{np+1}\right] \cdot \sin(np\theta) \cdot \left(\sum_{n=1}^{N_\lambda} \lambda_b \cdot \sin(nQ_s\theta)\right)
\end{aligned}
\tag{7}
$$

$$B_{s\theta I}(r,\theta) = \sum_{n=1,3,5\ldots}^{\infty} \frac{\mu_o M_n}{2\mu_r} \cdot \frac{np}{(np)^2-1} \cdot \left(\frac{2\left[\left(\frac{R_r}{R_m}\right)^{np+1} - \left(\frac{R_r}{R_m}\right)^{2np}\right]}{\frac{\mu_r+1}{\mu_r}\left[1-\left(\frac{R_r}{R_s}\right)^{2np}\right] - \frac{\mu_r-1}{\mu_r}\left[\left(\frac{R_m}{R_s}\right)^{2np} - \left(\frac{R_r}{R_m}\right)^{2np}\right]} \right) \cdot \left[-\left(\frac{r}{R_s}\right)^{np-1}\left(\frac{R_m}{R_s}\right)^{np+1} + \left(\frac{R_m}{r}\right)^{np+1} \right] \cdot \sin(np\theta) \cdot \left(\lambda_0 + \sum_{n=1}^{N_\lambda} \lambda_{an} \cdot \cos(nQ_s\theta) \right) - \sum_{n=1,3,5\ldots}^{\infty} \frac{\mu_o M_n}{2\mu_r} \cdot \frac{np}{(np)^2-1} \cdot \left(\frac{2\left[\left(\frac{R_r}{R_m}\right)^{np+1} - \left(\frac{R_r}{R_m}\right)^{2np}\right]}{\frac{\mu_r+1}{\mu_r}\left[1-\left(\frac{R_r}{R_s}\right)^{2np}\right] - \frac{\mu_r-1}{\mu_r}\left[\left(\frac{R_m}{R_s}\right)^{2np} - \left(\frac{R_r}{R_m}\right)^{2np}\right]} \right) \cdot \left[\left(\frac{r}{R_s}\right)^{np-1}\left(\frac{R_m}{R_s}\right)^{np+1} + \left(\frac{R_m}{r}\right)^{np+1} \right] \cdot \cos(np\theta) \cdot \left(\sum_{n=1}^{N_\lambda} \lambda_b \cdot \sin(nQ_s\theta) \right) \quad (8)$$

where M_n is the magnetization component for the permanent magnet, μ_r is the relative permeability, R_r is the rotor radius, R_m is the magnet radius, R_s is the stator inner radius, Q_s is the slot number, p is the pole-pair number, and μ_o is the permeability of the air. While λ_0, λ_{an}, and λ_b are the Fourier series coefficients of the complex relative permeance function (CRPF).

3. RESULTS AND ANALYSIS

3.1. Magnetic vector potential

It is important to ascertain that the flux patterns are correct as expected by field distributions in the permanent magnet. Applying the magneto-static analysis [21] which is available in the 2D finite element analysis (FEA), the open-circuit magnetic field distributions across the machine sectional area can be predicted as illustrated in Figure 4. Each machine is modelled with three different magnetization patterns for the surface-mounted rotor magnets i.e. radial magnetization (RM), parallel magnetization (PaM), and segmented Halbach magnetization (SH). The magnetic flux lines flow from one magnet to adjacent magnets with different polarities. Since this motor has four magnetic poles, there are four magnetic flux semi-circles in the rotor core.

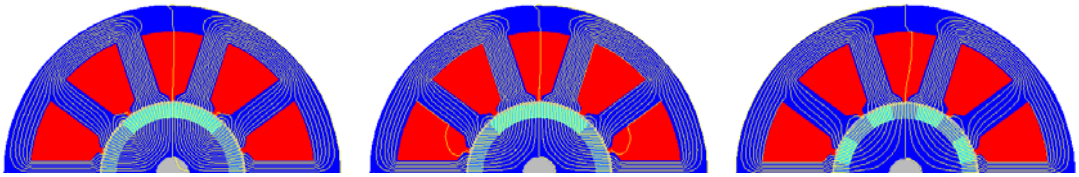

(a) PMSM with RM (b) PMSM with PaM (c) PMSM with SH

Figure 4. Magnetic field distributions during open-circuit for five-phase, 10-slot/4-pole PMSM under different magnetization patterns

3.2. Flux density distribution

The open-circuit flux density distributions for RM, PaM and SH magnetized magnets are computed from 2D FEA as shown in Figure 5. The highest values of magnetic flux density are 1.52T, 1.51T, and 1.55T for machines with RM, PaM and SH respectively. These highest values are observed mainly in the stator teeth and stator yoke. The magnetic flux density from the SH magnetization in the 10-slot/4-pole machine during open-circuit condition is the highest compared with the RM and PaM magnetization patterns. During on-load condition, the magnetic flux density in the machine is further influenced by the types of winding in the machine. Referring to Figure 6, it can be observed that the flux density is varied throughout the machine cross-sectional area. The PM machines are excited with sinusoidal phase current of 5A peak. Higher flux density inside tooth tip area is observed during the on-load operation. However, among these three winding configurations, DLDW produces the highest magnetic flux density as shown in Figure 6

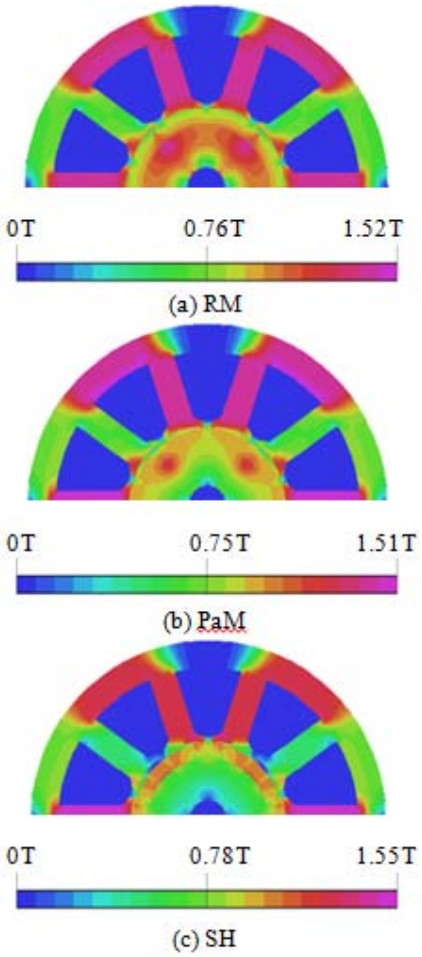

Figure 5. Contour of flux density distribution during open-circuit condition under different magnetization patterns

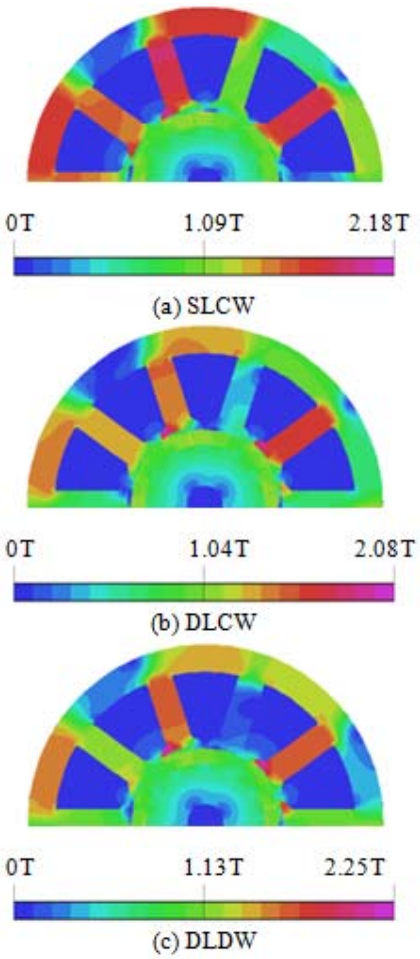

Figure 6. Contour of flux density distribution during on-load condition for SH under different winding configurations

Additionally, the airgap flux density distribution is one of the most important parameters to be optimized when designing PMSM. By using 2D FEA, the flux density distribution in the airgap can be computed for PMSMs with RM, PaM and SH as represented in Figure 7.

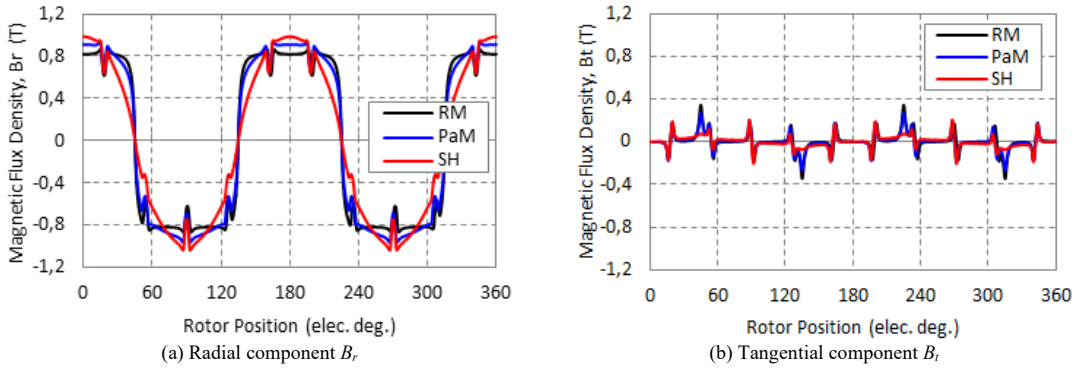

(a) Radial component B_r (b) Tangential component B_t

Figure 7. Flux density distributions in mid airgap (radius 25.5mm) under different magnetization patterns

3.3. Phase back-emf and harmonics

The phase back-emf waveforms of 10-slot/4-pole PMSMs for RM, PaM and SH are shown in Figure 8. It is noted that the phase back-emf for the machine with RM and PaM are trapezoidal in shape, but the machine with PaM exhibits slightly higher magnitude of phase back-emf than the machine with RM. Additionally, the phase back-emf for the machine with SH is more sinusoidal and higher in magnitude with DLDW compared to RM and PaM. Meanwhile, the machine with SLCW and DLCW configurations generate exactly the same magnitude and shape of phase back-emf.

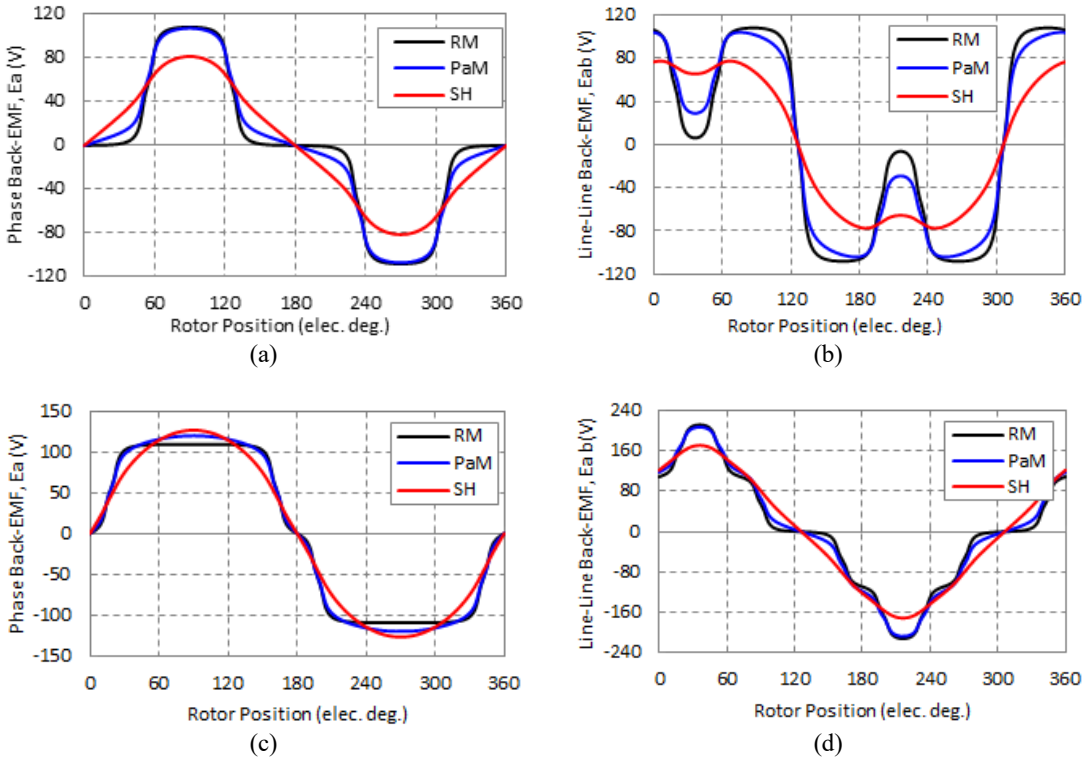

Figure 8. Phase and Line-Line back-emfs of five-phase, 10-slot/4-pole PMSM for different winding configurations and magnetization patterns, (a) Phase back-emf for SLCW and DLCW, (b) Line back-emf for SLCW and DLCW, (c) Phase back-emf for DLDW, (d) Line back-emf for DLDW

3.4. Cogging torque

Generally, cogging torque exists from the interaction of permanent magnet MMF harmonics and the air gap permeance harmonics due to slotting. A low cogging torque may be achieved when the ratio of the slot number to pole number is fractional, and the smallest common integer N_{scm} between the slot number and pole number is high. Since the PM machines under consideration have 10-slot/4-pole numbers, therefore, the smallest common integer N_{scm} is 20. As a result, the cogging torque waveform is repeating every 18^0 mech. or 36^0 elect. The system variable RMTORQUE in OPERA2D software computes the cogging torque when the machine is simulated during open-circuit condition as shown in Figure 9. As can be seen, both PM machines with PaM and RM have an almost similar shape of the cogging torque waveform. However, machine with PaM has slightly smaller cogging torque compared to machine with RM. As expected, a PM machine with SH exhibits almost zero cogging torque.

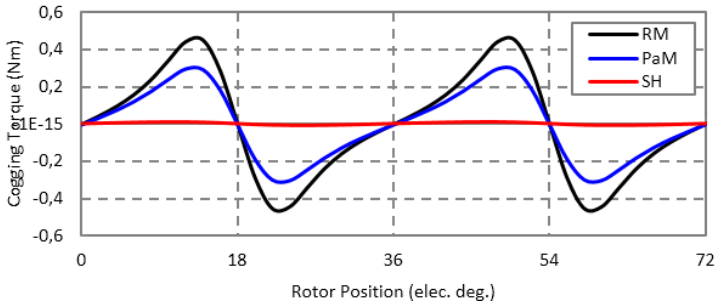

Figure 9. Cogging torque for five-phase ,10-slot/4-pole PMSM under different magnetization patterns

3.5. Electromagnetic torque

During the on-load condition, electromagnetic (EM) torque is simulated in 2D FEA rotating machine analysis by exciting phase currents of 5A peak into the stator windings. The EM torque waveforms of the five-phase, 10-slot/4-pole machine for three magnetization patterns are shown in Figure 10. The EM torque for the motor with PaM is the highest than RM and SH. The machine with SH has the lowest EM torque. This is quite expected since the fundamental back-emf is highest for the machine with PAM and lowest for SH, as shown earlier in Table 2. In addition, the machines with DLDW produces the highest EM torque, while the SLCW has a lowest EM torque value compared to other types of windings. Particularly, the torque ripple in the machines which have DLDW are the highest compared to others. The average EM torque and peak-to-peak torque ripple are listed in Table 3.

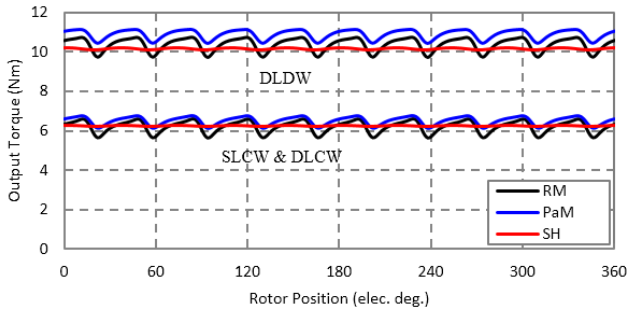

Figure 10. Electromagnetic torque for five-phase, 10-slot/4-pole PMSM under different magnetization patterns

Table 3. Electromagnetic torque with 5A sinusoidal phase current

Magnetization Patterns	Winding Configurations	Average EM Torque (Nm)	Peak-to-Peak Torque Ripple (Nm)	Peak-to-Peak Torque Ripple (%)
RM	SLCW	6.32	0.93	14.71
	DLCW	6.49	0.95	14.71
	DLDW	10.5	1.10	10.53
PaM	SLCW	6.59	0.72	10.97
	DLCW	6.78	0.68	10.09
	DLDW	10.9	0.82	7.59
SH	SLCW	6.13	0.025	0.42
	DLCW	6.24	0.029	0.46
	DLDW	10.1	0.10	0.99

3.6. Skewing method

The cogging torque in 10-slot/4-pole PMSM with RM and PaM can be further minimized by applying the skewing method in 2D FEA [22-25]. There is no more cogging torque minimization required for SH since it already exhibits almost zero cogging torque i.e. 0.04 Nm peak. Using OPERA2D software, the stator core

of 10-slot/4-pole PM machine has been sliced into three axial segments. Each axial segment of the stator is skewed with an inclination angle equal to 6º mechanical, making total skew angle α_i of 18º mechanical. Figure 11 shows the cogging torque reduction for the 10-slot/4-pole PM machine for RM and PaM respectively. The resultant cogging torque is nearly nine times smaller than the initial value. However, PM machine with skewed stator has slightly lower phase back-emf due to the skewing effect.

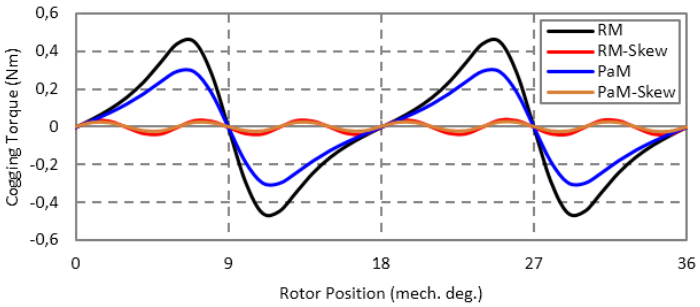

Figure 11. Cogging torque minimization using skewing method for five-phase, 10-slot/4-pole PMSM

4. CONCLUSION

This paper has investigated the influence of different winding configurations and magnetization patterns on the performance of a five-phase, 10-slot/4-pole PMSM. Generally, 10-slot/4-pole PMSM can produce different machine performance due to the differences in magnetization patterns and winding configurations. Further, it is also shown that better machine performance can be achieved by applying the skewing method in 2D FEA to minimize the cogging torque. In terms of phase back-emf, the machine with segmented Halbach exhibits the most sinusoidal waveform. Whereas, the PMSM with radial and parallel magnetizations induce more trapezoidal shape of phase back-emf. The five-phase, 10-slot/4-pole PMSM with double-layer distributed winding (DLDW) for parallel magnetization (PaM) gives the best machine performance compared to other types of machines, in terms of higher magnitude of fundamental phase back-emf, lower cogging torque, and higher electromagnetic torque. Future research will be focused on the torque versus speed of the PMSM in order to determine its suitability in the electric vehicles and hybrid electric vehicles.

ACKNOWLEDGEMENTS

The authors would like to thank Universiti Sains Malaysia for the financial support under RUI grant scheme with project number 1001/PELECT/8014027.

REFERENCES

[1] BP Energy Economics, 2018 BP Energy Outlook 2018 BP Energy Outlook, Available at: https://www.bp.com/content/dam/bp/en/corporate/pdf/energy-economics/energy-outlook/bp-energy-outlook-2018.pdf, 2018.
[2] A. M. Bazzi, Y. Liu & D. S. Fay, "Electric machines and energy storage: Over a century of technologies in electric and hybrid electric vehicles," *IEEE Electrification Magazine*, vol. 6(3), pp. 49-53, 2018.
[3] M. Zeraoulia, M. E. H. Benbouzid, & D. Diallo, "Electric Motor Drive Selection Issues for HEV Propulsion Systems: A Comparative Study, " *IEEE Transactions on Vehicular Technology*, vol. 55(6), pp. 1756-1764, 2006.
[4] Velev B., "Comparative Analysis of PMAC Motors for EV and HEV Applications," *Scientific Proceeding XXII International Scientific-Technical Conference (trans & MOTAUTO)*, vol. 2, pp. 78-82, 2014.
[5] N. K. Nguyen, et al., "Fault-tolerant operation of an open-end winding five-phase PMSM drive with short-circuit inverter fault," *IEEE Transactions on Industrial Electronics*, vol. 63(1), pp. 595-605, 2016.
[6] Feng Yu, et al., "Control and Performance Evaluation of Multiphase FSPM Motor in Low-Speed Region for Hybrid Electric Vehicles," *Energies*, vol. 8, pp. 10335-10353, 2015.
[7] D. Ting, L. Fenghui & S. Li, "Fault-tolerant method for six-phase PMSM by adjusting phase angle," *20th International Conference on Electrical Machines and Systems (ICEMS)*, pp. 1-5, Sydney, 2017.
[8] D. Ishak, Z. Q. Zhu, & D. Howe, "Comparative study of permanent magnet brushless motors with all teeth and alternative teeth windings," *Second IEE International Conference on Power Electronics, Machines, and Drives (PEMD)*, pp. 830-834. 2004.
[9] Ali Sarikhani, Wilder Saint-Hilaire, & Osama A. Mohammed, *A Study on the effect PM machine design parameters changes on performance measures*. IEEE PES General Meeting, 2010.

[10] S. Sadeghi and L. Parsa, "Multiobjective Design Optimization of Five Phase Halbach Array Permanent Magnet Machine, " *IEEE Transactions on Magnetics*, vol. 47(6), pp. 1658-1666, 2011.
[11] M. Rezal and D. Ishak, "New In-Wheel Electric Motor Design for Small Electric Vehicle Using Opera2D,"*Applied Mechanics and Materials*, vol. 165, pp. 38-42, 2012.
[12] B. Hannon, P. Sergeant & L. Dupré., "2-D Analytical Subdomain Model of a Slotted PMSM With Shielding Cylinder," *IEEE Transactions on Magnetics*, vol. 50(7), pp. 1-10, Jul 2014.
[13] A. Rahideh and T. Korakianitis., "Analytical magnetic field distribution of slotless brushless PM motors. Part 2: Open-circuit field and torque calculations," *IET Electrical Power Applications*, vol. 6(9), pp. 639, 2012.
[14] T. Lubin, S. Mezani & A. Rezzoug., "2-D exact analytical model for surface-mounted permanent-magnet motors with semi-closed slots," *IEEE Transactions on Magnetics*, vol. 47(2), pp. 479-492, Feb 2011.
[15] L. J. Wu, et al., "An improved subdomain model for predicting magneticf of surface-mounted permanent magnet machines accounting for tooth-tips," *in IEEE Transactions on Magnetics*, vol. 4 7(6), pp. 1693-1704, Jun 2011.
[16] Z. Q. Zhu, L. J. Wu & Z. P. Xia., "An accurate subdomain model for magnetic field computation in slotted surface-mounted permanent-magnet machines," *IEEE Transactions on Magnetics*, vol. 46(4), pp. 1100-1115, Apr 2010.
[17] A. Gilson, et al., "2-D analytical subdomain model for high-speed permanent-magnet machines," 18th International Conference on Electrical Machines and Systems (ICEMS), 2015, pp. 1508-1514, Pattaya, 2015.
[18] Tiang, T.L., et al., "A comprehensive analytical subdomain model and its field solutions for surface-mounted permanent magnet machines," *IEEE Transactions on Magnetics*, vol. SI(4), pp.1-14, Apr 2015.
[19] Z. Q. Zhu, D. Howe & C. C. Chan., "Improved analytical model for predicting the magnetic field distribution in brushless permanent-magnet machines," *IEEE Transactions on Magnetics*, vol. 38(1), pp. 229-238, Jan 2002.
[20] M. Rezal, D. Ishak & W. A. Salah., "Multiobjective design of permanent magnet synchronous machines based on analytical sub-domain particle swarm optimization," *IEEE Conference on Energy Conversion (CENCON)*, pp. 230-235, Kuala Lumpur, 2017.
[21] M. Rezal, et al., "Static Analysis of 18-Slot/16-Pole Permanent Magnet Synchronous Motor Using FEA," *International Journal of Engineering and Technology*, vol. 5(3), pp. 176-180, 2015.
[22] Goga Cvetkovski, Lidija Petrovska, & Paul Lefley., "Topological modifications in function of cogging torque reduction of permanent magnet synchronous motor," *Przeglad Electrotechniczny*, pp. 113-115, 2014.
[23] L. Melcescu, M. Covrig & A. Moraru., "Analyses of core skewing influence in permanent magnet synchronous machine by 2D FEM field computation," *U. P. B. Sci. Bull. , Series C*, vol. 68(2), pp. 41-52, 2006.
[24] O. Kudrjavtsev and A. Kilk., "Cogging torque reduction methods," *Electrical Power Quality Supply Reliability Conference*, pp. 251-254, 2014
[25] Rihab Abdelmoula, et al., "Reducing torque ripple in permanent magnet synchronous motor," *Journal of Electrical Systems*, vol. 13(3), pp. 528-542, 2017.

BIOGRAPHIES OF AUTHORS

Mohd Rezal Mohamed received the BEng (Hons) degree in electrical and electronics engineering and the MSc in electronic engineering from the Universiti Putra Malaysia, Serdang, Selangor, Malaysia in 2002 and 2008 respectively. He is currently pursuing PhD degree in electrical machines and drives from the Universiti Sains Malaysia, Penang, Malaysia. He is currently a senior lecturer at the Electrical, Electronics, and Automation Section, Universiti Kuala Lumpur, Malaysian Spanish Institute, Kulim, Kedah, Malaysia. His current research interests include design of permanent magnet synchronous machines and electric vehicles.

Dahaman Ishak received the BSc degree in electrical engineering from Syracuse University, Syracuse, NY, USA, the MSc degree in electrical power from the University of Newcastle Upon Tyne, Newcastle upon Tyne, UK, and the PhD degree in electrical engineering from the University of Sheffield, Sheffield, UK, in 1990, 2001 and 2005 respectively. He is currently an Associate Professor with the School of Electrical and Electronic Engineering, Universiti Sains Malaysia, Penang, Malaysia. His current research interests include permanent magnet brushless machines, electrical drives, power electronic converters and renewable energy.